Organic & Biomolecular Chemistry

PAPER

View Article Online
View Journal | View Issue

Cite this: *Org. Biomol. Chem.*, 2015, **13**, 10198

Synthesis and electronic properties of π-extended flavins†

L. N. Mataranga-Popa,[a,b] I. Torje,[b] T. Ghosh,[a] M. J. Leitl,[a] A. Späth,[a] M. L. Novianti,[c] R. D. Webster*[c] and B. König*[a]

Received 12th July 2015,
Accepted 14th August 2015

DOI: 10.1039/c5ob01418b

www.rsc.org/obc

Flavin derivatives with an extended π-conjugation were synthesized in moderate to good yields from aryl bromides *via* a Buchwald–Hartwig palladium catalyzed amination protocol, followed by condensation of the corresponding aromatic amines with violuric acid. The electronic properties of the new compounds were investigated by absorption and emission spectroscopy, cyclic voltammetry, density functional theory (DFT) and time dependent density functional theory (TDDFT). The compounds absorb up to 550 nm and show strong luminescence. The photoluminescence quantum yields ϕ_{PL} measured in dichloromethane reach 80% and in PMMA (poly(methyl methacrylate)) 77%, respectively, at ambient temperature. The electrochemical redox behaviour of π-extended flavins follows the mechanism previously described for the parent flavin.

Flavins are the prosthetic group of flavoproteins and universal redox cofactors in biology.[1–3] They play an important role in light, oxygen, and voltage-sensitive (LOV) domains sensitive for blue light excitation.[4] However, flavins have also found many applications in photocatalysis[5–11] or as photosensitizers[12–14] in singlet oxygen generation for synthesis or in photodynamic disinfection.[13,15,16] The local environment,[17] hydrogen bonding,[18,19] π–π stacking[20] or metal coordination[21,22] to the chromophore and the type and position of substituents[23] determine the redox potentials and the photophysical properties of flavin derivatives. Donor–acceptor systems, in which flavins are covalently linked to other chromophores showing different absorptions have been synthesized[24,25] and used in photo-voltaic devices,[26] molecular switching or molecular logic gates.[26,27] Oxidized forms of flavin derivatives act as electron acceptors in photoinduced electron transfer (PET)[28,29] and are known to bind different metal ions inducing a positive shift in their one-electron reduction potentials[29] and long-lived charge-separation.[29]

A less explored option to modify the optical and electronic properties of flavins is the extension of their aromatic π-system. An extended conjugation length is expected to shift the absorption maxima to a longer wavelength and affect the extinction coefficient and redox properties of the chromophore.[30,31] We report here the synthesis and electronic properties of three new flavins with extended aromatic π-systems.

Results and discussion

Synthesis

The synthesis of new π-system extended flavins **3a**, **3b** and **3c**[32] was accomplished by the condensation[33] of violuric acid **1** with the corresponding amines **2a–c** as starting materials. The amines were obtained *via* a Buchwald–Hartwig amination[34] in good to very good yields. The subsequent condensation of amines **2a–2c** with violuric acid **1** in boiling acetic acid easily furnished multi-gram quantities of flavins **3a–c** in moderate to good yields (Scheme 1).

The structures of flavins **3a–3c** were determined by NMR spectroscopy and confirmed by high resolution mass spectrometry and elemental analysis. The electronic properties of flavin derivatives **3a–3c** were investigated by absorption and emission spectroscopy (Table 1), cyclic voltammetry, DFT and TDDFT calculations (Fig. 1). Furthermore, the fluorescence quantum yields of the chromophores were determined with an integrating sphere accessory.

Theoretical calculations

Computational investigations are particularly useful for understanding trends observed in the electrochemical and photophysical properties of molecular materials. Thus, density functional theory (DFT) and time dependent density func-

[a]*University of Regensburg, Universitatsstraße 31, 93053 Regensburg, Germany. E-mail: burkhard.koenig@chemie.uni-regensburg.de*
[b]*Babes-Bolyai University Cluj-Napoca, Faculty of Chemistry and Chemical Engineering, Arany Janos Str. 11, Cluj-Napoca, 400428 Romania*
[c]*Division of Chemistry & Biological Chemistry, School of Physical and Mathematical Sciences, Nanyang Technological University, 21 Nanyang Link, 637371 Singapore. E-mail: Webster@ntu.edu.sg*

†Electronic supplementary information (ESI) available: Detailed experimental procedures, copies of ^{1}H and ^{13}C NMR spectra of compounds **2a–2c** and **3a–3c**; and selected molecular orbitals for compounds **3a–3c**. See DOI: 10.1039/c5ob01418b

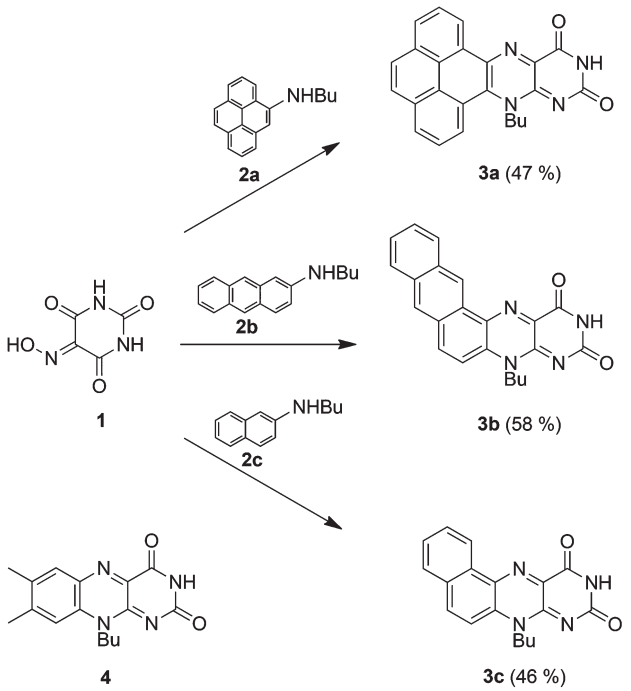

Scheme 1 Synthesis of the flavins **3a–3c**. Reaction conditions: amines **2a–2c** (1.2 eq.), violuric acid **1** (1 eq.), acetic acid, reflux, 19 h. For comparison, the structure of the parent flavin **4** is shown.

tional (TDDFT) calculations were performed to gain additional understanding of the electronic structures of the π-expanded flavins (**3a**, **3b**, and **3c**).

Interestingly, the contour curves of the lowest unoccupied molecular orbitals (LUMOs) look similar for all three investigated compounds being largely unaffected by the π-extension (Fig. 1). Also, the LUMO energies are similar ranging from −2.88 eV to −2.96 eV. In contrast to this, the highest occupied molecular orbitals (HOMOs) are delocalized over large parts of the molecule for all investigated compounds (Fig. 1). Consequently, the HOMO energies vary in a wider energy range from −5.70 eV to −6.11 eV.

TDDFT calculations revealed that transitions between these frontier orbitals determine the lowest excited singlet state S_1. The corresponding transition energies amount to 2.47 eV (**3a**), 2.44 eV (**3b**), and 2.85 eV (**3c**). This is in agreement with the experimental results (see below) which show that the emission energies of compounds **3a** and **3b** are similar, whereas the emission of compound **3c** is clearly blue-shifted. This trend is also seen in the absorption spectra.

Electronic properties

The UV-visible absorption and emission spectral data of the flavins in two different organic solvents and in a polymer matrix (PMMA = poly(methyl methacrylate)) are summarized in Table 1. The absorption and emission spectra of flavin derivatives **3a**, **3b**, **3c**, and butyl flavin derivative **4** recorded in DMSO are displayed in Fig. 2a and b. All new derivatives show a complex absorption profile characteristic for the presence of multiple chromophores. The flavins exhibit intense absorption bands in the range of 306–543 nm. The $S_0 \rightarrow S_1$ band around 440 nm, characteristic for the parent flavin **4**, is red shifted by 15 nm for compound **3c**, 52 nm for **3b**, and 57 nm for **3a**, respectively, in DMSO solution, indicating a decreased HOMO–LUMO gap. Furthermore, the absorption bands in the range 306–400 nm show a vibrational fine structure characteristic for the isolated naphthalene, anthracene and pyrene chromophore.[35] However, the molar extinction coefficient of anthracene derivative **3b** is significantly higher than those observed for pyrene **3a** and naphthalene **3c**. A likely reason for this is the extended linear conjugated system.

Compounds **3a** and **3b** show an intense orange emission under daylight irradiation, while **3c** emits in the green.

The emission spectrum of **3c** shows a vibrational structure, similar to that of butyl flavin (**4**), with a spacing of the vibrational satellites amounting to about 1000 cm^{-1}. This energy spacing corresponds to the characteristic stretching modes of isoalloxazines. Furthermore, the structured emission indicates that the emission is originating from a localized π–π* transition. In contrast, the emissions of **3a** and **3b** are broad and do not exhibit any structure indicating that the emission originates from a state with some charge transfer character.

Table 1 Selected photophysical properties of flavins **3a–3c** and **4** measured at ambient and liquid nitrogen temperature, respectively. $\lambda_{abs.max}$ is the peak wavelength of the absorption spectrum, $\lambda_{em.max}$ is the peak wavelength of the emission spectrum, τ the emission decay time, and Φ_{PL} the photoluminescence quantum yield. PMMA: poly(methyl methacrylate)

Compound	Solvent polymer	$\lambda_{abs.max}$ [nm]	$\lambda_{em.max}$ (300 K) [nm]	τ (300 K)/τ (77 K) [ns]	Φ_{PL} (300 K)/Φ_{PL} (77 K) [%]
3a	DCM	339, 355, 503, **543**	610		60/80
	DMSO	340, 357, 500, **530**	628	9/15	46/57
	PMMA		580	11/11	50/74
3b	DCM	361, 384, 505, **542**	585		24/70
	DMSO	357, 386, 495, **526**	605	7/16	53/65
	PMMA		628	6/6	28/35
3c	DCM	306, **462**, 490	511, 544 (sh)		80/≈100
	DMSO	306, **457**, 486	516, 545 (sh)	2/11	13/33
	PMMA		518 (sh), 539	11/11	77/80
4	DMSO	343, **443**, 470	498, 526 (sh)	—	14

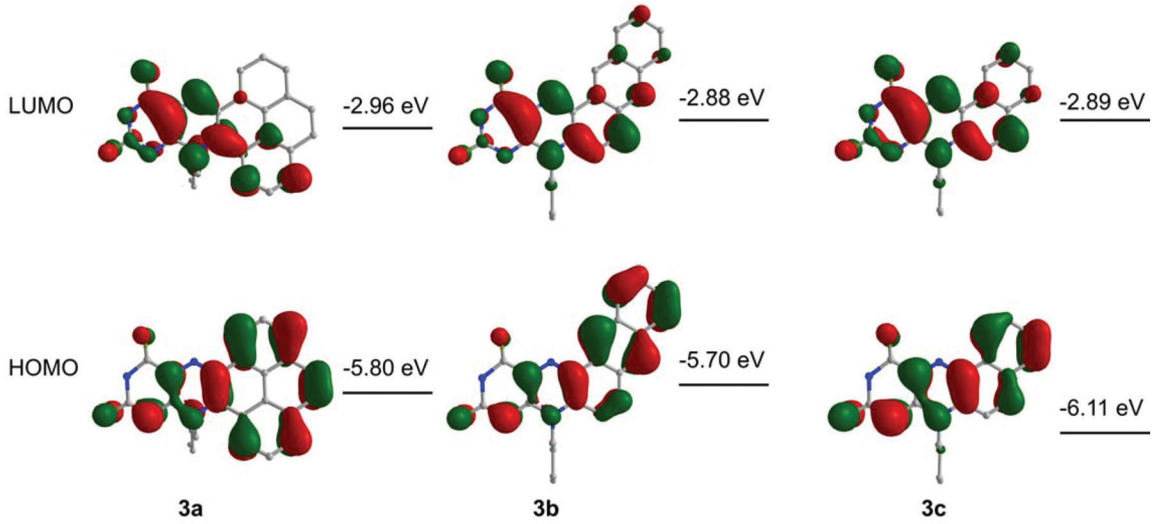

Fig. 1 HOMOs and LUMOs of compounds **3a**, **3b**, and **3c**. The plots result from DFT calculations performed on the B3LYP/6-31G** level of theory. The iso-contour value was set to 0.03. Further molecular orbitals and the corresponding energies are displayed in the ESI.†

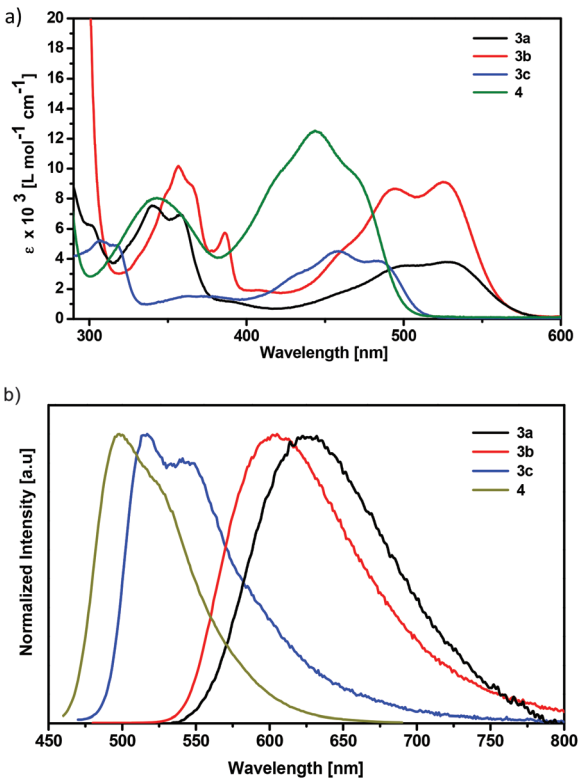

Fig. 2 (a) UV-Vis and (b) emission spectra of 1.0×10^{-4} M solutions of **3a** (black line), **3b** (red line), **3c** (blue line) and **4** (green line) in DMSO at 300 K (λ_{exc} = 450 nm).

This assignment is also supported by the TDDFT calculation (Fig. 1), which predicts that the S_1 state is of partial charge transfer character for **3a** and **3b** due to HOMO orbitals delocalized over the entire molecule and LUMO orbitals localized on the isoalloxazine part. In addition, the emission maxima show a clear dependence on the polarity of the solvent, which is typical for charge transfer transitions. In the case of **3a**, in DCM (ET(30) = 41.1)[36] the emission peaks at 610 nm whereas it is red shifted by 18 nm in DMSO (ET(30) = 45.0)[36] to 628 nm. Compound **3b** exhibits a similar red shift of 20 nm from 585 nm to 605 nm when we go from DCM to DMSO. For flavin **3c** a corresponding shift from 511 nm to 516 nm is observed.

The emission quantum yields of the new compounds **3a–3c** vary with solvent and temperature. In solution at T = 300 K the emission quantum yields are between 24 and 80% in DCM, 13 and 53% in DMSO and 13 and 77% in PMMA. The corresponding Φ_{PL} values at nitrogen temperature increase, which may be explained by a decrease of non-radiative deactivations on cooling. The life times at 300 K of the excited states of the three compounds are in the range of 2 to 9 ns in DMSO and 6–11 ns in PMMA. The values increase only slightly when decreasing the temperature from 300 K to 77 K; in PMMA the same values are observed for both temperatures. We assume that the radiative emission at 300 K and 77 K originates from the singlet excited state being involved without the triplet state involvement.

Redox properties

The voltammetric behaviour and reduction mechanism of compounds **3a**, **3b** and **3c** in DMSO can be interpreted based on the mechanism for the closely related riboflavin, which has been studied in detail previously.[37–39]

The variable scan rate cyclic voltammograms of compound **3a** shown in Fig. 3 appear most similar to those obtained for riboflavin and can be interpreted based on the mechanism in Scheme 2.[39] Compound **3a** (Fl_{ox}) is initially reduced at $E^0_{f(1)}$ by one-electron to form the radical anion ($Fl_{rad}^{\bullet -}$). The radical anion reacts quickly with another flavin by proton transfer to

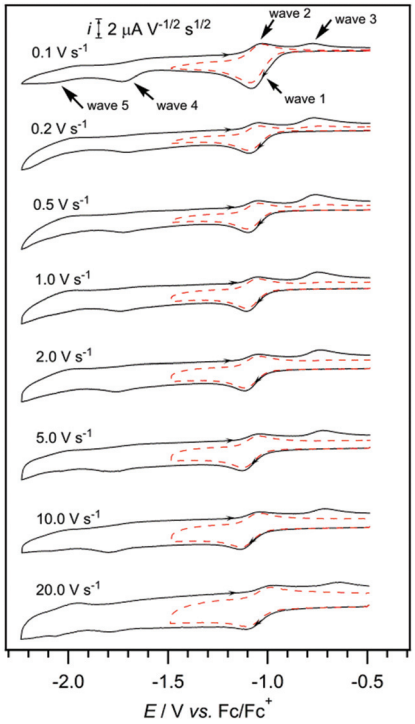

Fig. 3 Variable scan rate CVs of 2 mM **3a** in DMSO with 0.2 M n-Bu_4NPF_6, recorded at a 1 mm Pt electrode at 22(±2) °C. The current data were scaled by multiplying by $\nu^{-0.5}$.

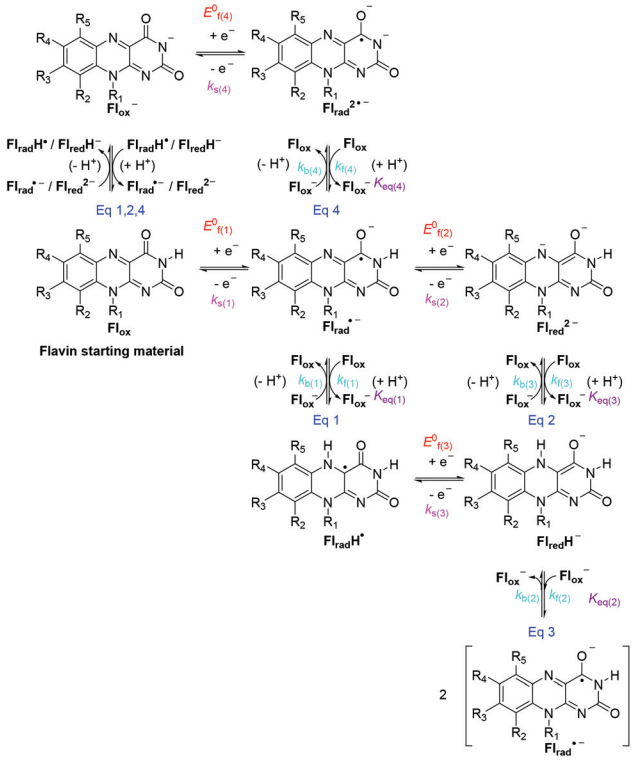

Scheme 2 General electrochemical reduction mechanism for flavins in DMSO.

form the neutral radical ($Fl_{rad}H^{\bullet}$) *via* eqn (1) plus the deprotonated flavin (Fl_{ox}^{-}). Because $Fl_{rad}H^{\bullet}$ is easier to reduce than Fl_{ox}, it is immediately further reduced at the electrode surface by one-electron to form $Fl_{red}H^{-}$ at $E^0_{f(3)}$. Therefore, the first voltammetric process (wave 1) observed at ~−1.0 V *vs.* Fc/Fc^{+} actually involves two one-electron transfers interspaced with a proton transfer reaction. When the scan direction is reversed at approximately −1.5 V *vs.* Fc/Fc^{+}, two oxidative peaks are observed. The first oxidative peak at ~−1.0 V *vs.* Fc/Fc^{+} (wave 2) is due to the one-electron oxidation of $Fl_{rad}^{\bullet-}$ back to the starting material, Fl_{ox}, while the second electron transfer at −0.7 V *vs.* Fc/Fc^{+} is due to the one-electron oxidation of $Fl_{red}H^{-}$ to $Fl_{rad}H^{\bullet}$ (wave 3). If the equilibrium in eqn (1) in Scheme 2 favours the back reaction (as it does for riboflavin),[39] then any $Fl_{rad}H^{\bullet}$ that deprotonates on the voltammetric timescale will also undergo further one-electron oxidation in wave 3 to regenerate the starting material. As the scan rate is increased up to 20 V s^{-1}, the initial reduction process at ~−1.0 V *vs.* Fc/Fc^{+} becomes more chemically reversible shown by how the i_p^{ox}/i_p^{red} ratio approaches unity, due to the proton transfer step between $Fl_{rad}^{\bullet-}$ and Fl_{ox} being outrun; hence the reduction process changes to a chemically reversible one-electron transfer.

When the voltammetric scan is extended to more negative potentials, additional reduction processes are detected at ~−1.7 V *vs.* Fc/Fc^{+} (wave 4) and ~−2.0 V *vs.* Fc/Fc^{+} (wave 5) for compound **3a**. Wave 4 is associated with the one-electron reduction of Fl_{ox}^{-} that is formed from the Fl_{ox} reacting with $Fl_{rad}^{\bullet-}$ ($E^0_{f(4)}$), and wave 5 is associated with the further one-electron reduction of $Fl_{rad}^{\bullet-}$ to form Fl_{red}^{2-} ($E^0_{f(5)}$). When the forward potential scan is extended all the way past wave 5, on the reverse scan it can be observed that the oxidative wave 3 is larger than when the forward scan is only extended just past wave 1. The reason for wave 3 appearing larger is because $Fl_{red}H^{-}$ (which undergoes oxidation in wave 3) can also be formed *via* Fl_{red}^{2-} reacting with Fl_{ox} to form $Fl_{red}H^{-}$ (plus Fl_{ox}^{-}) (eqn (2)).

The voltammetric responses observed for compounds **3b** and **3c** appear somewhat different from **3a**, but they can be interpreted based on exactly the same mechanism as for compound **3a**; the subtle differences in the voltammetric waves can be accounted for by varying equilibrium constants for the homogeneous reactions given in Scheme 2. For example, at relatively slow scan rates the first voltammetric reduction process of **3b** and **3c** appears to be fully chemically reversible implying a simple chemically reversible electron transfer reaction (only waves 1 and 2 are observed), and the process remains chemically reversible as the scan rate is increased up to 20 V s^{-1}. The reason for the high chemical reversibility likely relates to the radical anion ($Fl_{rad}^{\bullet-}$) formed in the initial electron transfer step at $E^0_{f(1)}$ undergoing a slow homogeneous reaction with Fl_{ox} (eqn (1)), so on the short voltammetric timescale $Fl_{rad}^{\bullet-}$ survives fully at the electrode surface and is able to be converted back to Fl_{ox} when the scan direction is reversed (Fig. 4 and 5).

When the scan is extended to more negative potentials, compounds **3b** and **3c** show an additional process at ~−1.8 V

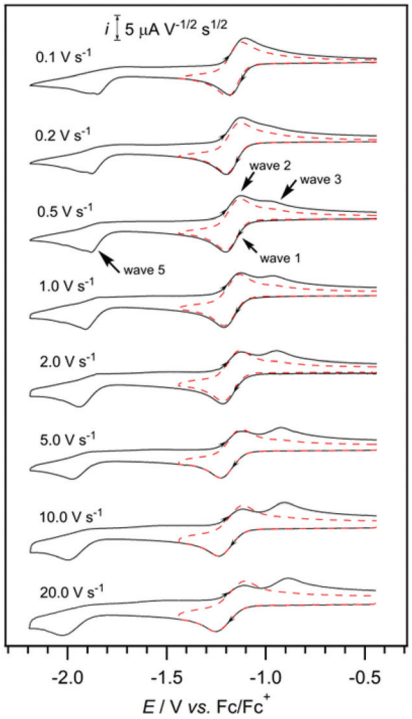

Fig. 4 Variable scan rate CVs of 2 mM **3b** in DMSO with 0.2 M n-Bu_4NPF_6, recorded at a 1 mm Pt electrode at 22(±2) °C. The current data were scaled by multiplying by $\nu^{-0.5}$.

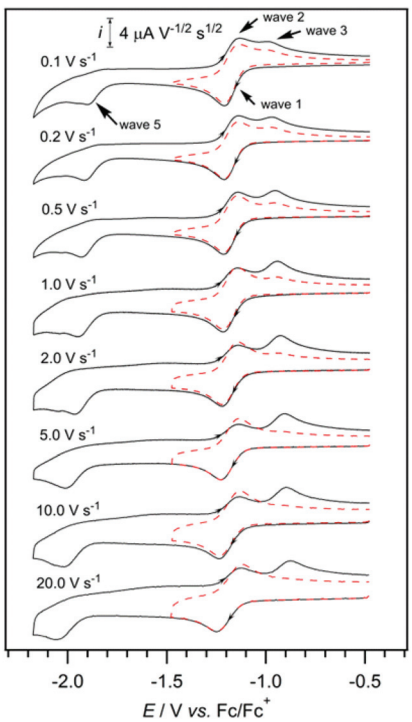

Fig. 5 Variable scan rate CVs of 2 mM **3c** in DMSO with 0.2 M n-Bu_4NPF_6, recorded at a 1 mm Pt electrode at 22(±2) °C. The current data were scaled by multiplying by $\nu^{-0.5}$.

vs. Fc/Fc^+ (wave 5) which is associated with the further one-electron reduction of $Fl_{rad}^{\bullet-}$ to form Fl_{red}^{2-} ($E^0_{f(5)}$). Wave 5 appears more clearly than was observed during the reduction of compound **3a** because more $Fl_{rad}^{\bullet-}$ exists at the electrode surface in higher amounts (due to the slower proton transfer reaction with Fl_{ox}). Similarly, the reduction process associated with wave 4 ($E^0_{f(4)}$) is not observed during the reduction of **3b** and **3c** because Fl_{ox}^- does not have time to form *via* the proton transfer reaction between $Fl_{rad}^{\bullet-}$ and Fl_{ox}. The peak shape of the wave 5 reduction process is "sharp" and this is likely due to some adsorption of the dianion onto the electrode surface. The reason that wave 4 (reduction of $Fl_{red}H^-$ to $Fl_{rad}^{2\bullet-}$) is not observed for compounds **3b** and **3c** may arise either due to lower acidity of the N–H proton of the starting materials or due to lower basicity of their corresponding anion radicals ($Fl_{rad}^{\bullet-}$).

When then voltammetric scanning direction was switched at −2.2 V *vs.* Fc/Fc^+ after first reducing $Fl_{rad}^{\bullet-}$ to Fl_{red}^{2-}, no reverse peak was detected associated with the oxidation of Fl_{red}^{2-} back to $Fl_{rad}^{\bullet-}$ regardless of the scan rate, indicating that the dianion is only very short-lived for compounds **3b** and **3c**. Similarly, when the potential was first scanned to −2.2 V *vs.* Fc/Fc^+, on the reverse scan only wave 2 was observed at slow scan rates. However, as the scan rate is increased, wave 3 becomes more pronounced and wave 2 diminishes in size. A reason for this apparently anomalous behaviour can be based on the equilibrium reactions that exist between the different species in Scheme 2 favouring the reformation of $Fl_{rad}^{\bullet-}$. For example, when the dianion is formed, it immediately undergoes a proton transfer reaction with the starting material to form $Fl_{red}H^-$ plus Fl_{ox}^- (Scheme 2, eqn (2)). $Fl_{red}H^-$ then undergoes another reaction with Fl_{ox}^- to form two molecules of $Fl_{rad}^{\bullet-}$ (Scheme 2, eqn (3)). Therefore, at slow scan rates, Fl_{red}^{2-} has time to convert all the way back to $Fl_{rad}^{\bullet-}$ so only wave 2 is observed, while at faster scan rates, there is only time for Fl_{red}^{2-} to convert to $Fl_{red}H^-$ and so wave 3 is mainly observed.

Experimental part

Computational procedures

DFT and TDDFT calculations were performed using Gaussian 09.[40] For all calculations (geometry optimizations and TDDFT energy calculations), B3LYP[41,42] was used as the functional in combination with the 6-31G** basis set.[43,44] As the starting geometry, manually drawn structures were used. For all compounds, the structure was optimized prior to TDDFT energy calculations.

General procedure for the syntheses of compounds 3a–c (GP1)

A mixture of amines **2a–c** (1 eq.), violuric acid **1** (1.2 eq.) and 100 mL of glacial acetic acid was added to a round bottom flask and refluxed for 24 h. Acetic acid was removed under reduced pressure, giving a purple solid residue. The residue was purified by flash chromatography on silica gel

(chloroform/methanol 50 : 1) to yield flavins **3a–c** as yellow or red solids.

9-Butylpyreno[4,5-*g*]pteridine-11,13(9*H*,12*H*)-dione (3a)

This compound was synthesized according to **GP1** and after purification by flash chromatography on silica gel (chloroform/methanol 50 : 1), **3a** (224 mg, 47%) was obtained as a red solid. R_f (chloroform/methanol 10 : 1): 0.44.

M.p. 300 °C (decomp). ^{1}H-NMR (300 MHz, CF_3COOD, δ ppm): 1.43 (t, J = 6 Hz, 3 H), 1.92 (m, 2 H), 2.76 (m, 2 H), 6.19 (t, J = 6 Hz, 2 H), 8.76 (m, 4 H), 9.05 (d, J = 9 Hz, H), 9.24 (d, J = 9 Hz, H), 9.45 (d, J = 9 Hz, H), 9.99 (d, J = 9 Hz, H). ^{13}C-NMR (300 MHz, CF_3COOD, δ ppm): 11.69 (CH_3), 18.91 (CH_2), 30.47 (CH_2), 59.46 (CH_2), 109.07 (CH), 112.82 (C_{quat}), 116.57 (C_{quat}), 120.32 (CH), 124.93 (CH), 125.64 (CH), 126.94 (CH), 127.45 (CH), 129.21 (C_{quat}), 129.45 (CH), 129.93 (CH), 130.26 (C_{quat}), 132.11 (C_{quat}), 132.36 (C_{quat}), 133.21 (C_{quat}), 136.86 (C_{quat}), 140.18 (C_{quat}), 141.75 (C_{quat}), 144.86 (C_{quat}), 150.12 (C_{quat}). IR (ν, cm^{-1}): 2961 (m), 1652 (s), 1460 (m), 1426 (m), 1400 (m), 1191 (m). UV-Vis (CH_2Cl_2): $\lambda_{max}(\varepsilon)$ = 281 (17 100), 340 (8480), 355 (8250), 503 (3740), 543 (4370). MS (ES-MS) m/z: 395 (M^+ + H). MS(HRMS/ESI) m/z: calc. For $C_{24}H_{18}N_4O_2$ (M^+ + H): 395.143, found 395.150. Anal. calcd for $C_{24}H_{18}N_4O_2 \cdot 0.5H_2O$: C 71.45, H 4.75, N 13.89, found: C 71.02, H 4.60, N 13.91.

5-Butylanthra[1,2-*g*]pteridine-1,3(2*H*,5*H*)-dione (3b)

The compound was synthesized according to **GP1** and after purification by flash chromatography on silica gel (chloroform/methanol 50 : 1), **3b** (224 mg, 58%) was obtained as a red solid. R_f (chloroform/methanol 10 : 1): 0.20.

M.p. 320 °C (decomp). ^{1}H-NMR (300 MHz, CF_3COOD, δ ppm): 1.69 (t, J = 6 Hz, 3 H), 2.36 (m, 2 H), 2.71 (m, 2 H), 5.57 (t, J = 9 Hz, 2 H), 8.44 (m, 3 H), 8.85 (dd, J = 6 Hz, 2 H), 9.31 (s, H), 9.50 (d, J = 9 Hz, H), 10.47 (s, H). ^{13}C-NMR (300 MHz, CF_3COOD, δ ppm): 12.06 (CH_3), 19.36 (CH_2), 29.81 (CH_2), 51.32 (CH_2), 109.06 (CH), 112.81 (C_{quat}), 116.56 (CH), 120.32 (CH), 126.00 (CH), 127.22 (CH), 129.23 (C_{quat}), 129.74 (CH), 129.90 (C_{quat}), 130.49 (C_{quat}), 132.10 (CH), 143.96 (CH), 135.35 (C_{quat}), 136.78 (C_{quat}), 140.06 (C_{quat}), 143.76 (C_{quat}), 150.15 (C_{quat}), 150.49 (C_{quat}). IR (ν, cm^{-1}): 2958 (m), 1647 (s), 1518 (m), 1496 (m), 1448 (m), 1244 (m). UV-Vis (CH_2Cl_2): $\lambda_{max}(\varepsilon)$ = 295 (27 210), 361 (6900), 505 (5940), 542 (7210). MS (ES-MS) m/z: 371 (M^+ + H). MS (HRMS/ESI) m/z: calc. For $C_{22}H_{18}N_4O_2$ (M^+ + H): 371.1503, found 371.1506.

7-Butylnaphto[1,2-*g*]pteridine-9,11(7*H*,10*H*)-dione (3c)[32]

The compound was synthesized according to **GP1** and after purification by recrystallization from chloroform, **3c** (173 mg, 46%) was obtained as an orange solid. R_f (chloroform/methanol 10 : 1): 0.38.

M.p. 280 °C (decomp). ^{1}H-NMR (300 MHz, CF_3COOD, δ ppm): 1.80 (t, J = 6 Hz, 3 H), 2.47 (m, 2 H), 2.82 (m, 2 H), 5.74 (t, J = 6 Hz, 2 H), 8.85 (m, 4 H), 9.55 (d, J = 9 Hz, H), 10.1 (d, J = 6 Hz, H). ^{13}C-NMR (300 MHz, CF_3COOD, δ ppm): 12.16 (CH_3), 19.48 (CH_2), 29.92 (CH_2), 51.41 (CH_2), 109.18 (CH), 112.93 (CH), 116.68 (CH), 120.44 (CH), 125.40 (CH), 129.00 (CH), 130.14 (C_{quat}), 130.65 (C_{quat}), 132.98 (C_{quat}), 133.50 (C_{quat}), 133.70 (C_{quat}), 140.59 (C_{quat}), 141.53 (C_{quat}), 147.61 (C_{quat}). IR (ν, cm^{-1}): 2967 (w), 1638 (s), 1473 (m), 1412 (s), 1202 (m). UV-Vis (CH_2Cl_2): λ_{max} (ε) = 262 (18 440), 306 (8170), 315 (8350), 434 (5280), 462 (8210), 490 (7080). MS (ES-MS) m/z: 321 (M^+ + H). MS(HRMS/ESI) m/z: calc. For $C_{18}H_{16}N_4O_2$ ($M + H^+$): 321.1273, found 321.1350.

Conclusions

Flavin derivatives **3a–c** were obtained from the condensation of naphthyl-, anthranyl- or pyrenyl-amines **2a–c** with violuric acid. Extending the π-system of the parent flavin by annulation of benzene, the naphthalene or pyrene unit changes the electronic and redox properties of the chromophore significantly. The chromophore absorption shifts bathochromic and all three compounds show intensive emission with quantum yields of up to 80%. The reduction mechanism of the expanded flavins in DMSO as observed in cyclic voltammetry experiments can be interpreted analogously to the previously investigated parent flavin, with the subtle differences in the voltammetric behaviour due to varying equilibrium constants for the homogeneous reactions following electron transfer.

Acknowledgements

We thank M. Hansen for helping with the graphical abstract.

Notes and references

1 J. P. Beardmore, L. M. Antill and J. R. Woodward, *Angew. Chem., Int. Ed.*, 2015, **54**, 8494–8497.
2 E. Jortzik, L. Wang, J. Ma and K. Becker, in *Flavins and Flavoproteins*, ed. S. Weber and E. Schleicher, Springer, New York, 2014, vol. 1146, ch. 7, pp. 113–157.
3 M. Lee, J. Hong, D.-H. Seo, D. H. Nam, K. T. Nam, K. Kang and C. B. Park, *Angew. Chem., Int. Ed.*, 2013, **52**, 8322–8328.
4 K. S. Conrad, C. C. Manahan and B. R. Crane, *Nat. Chem. Biol.*, 2014, **10**, 801–809.
5 V. Mojr, E. Svobodova, K. Strakova, T. Nevesely, J. Chudoba, H. Dvorakova and R. Cibulka, *Chem. Commun.*, 2015, **51**, 12036–12039.
6 S. K. B. König and R. Cibulka, *Chemical Photocatalysis*, ed. B. König, de Gruyter, Berlin, 2013, pp. 45–66.
7 J. Daďová, S. Kümmel, C. Feldmeier, J. Cibulková, R. Pažout, J. Maixner, R. M. Gschwind, B. König and R. Cibulka, *Chem. – Eur. J.*, 2013, **19**, 1066–1075.
8 T. Ghosh, T. Slanina and B. Konig, *Chem. Sci.*, 2015, **6**, 2027–2034.
9 R. Lechner, S. Kummel and B. Konig, *Photochem. Photobiol. Sci.*, 2010, **9**, 1367–1377.
10 U. Megerle, M. Wenninger, R.-J. Kutta, R. Lechner, B. Konig, B. Dick and E. Riedle, *Phys. Chem. Chem. Phys.*, 2011, **13**, 8869–8880.

11 B. Muhldorf and R. Wolf, *Chem. Commun.*, 2015, **51**, 8425–8428.
12 D. R. Cardoso, S. H. Libardi and L. H. Skibsted, *Food Funct.*, 2012, **3**, 487–502.
13 B. G. Solheim, *Transfus. Apher. Sci.*, 2008, **39**, 75–82.
14 R. Yin, T. Dai, P. Avci, A. E. S. Jorge, W. C. M. A. de Melo, D. Vecchio, Y.-Y. Huang, A. Gupta and M. R. Hamblin, *Curr. Opin. Pharmacol.*, 2013, **13**, 731–762.
15 J. Glaeser, A. M. Nuss, B. A. Berghoff and G. Klug, in *Advances in Microbial Physiology*, ed. K. P. Robert, Academic Press, 2011, vol. 58, pp. 141–173.
16 M. Insińska-Rak and M. Sikorski, *Chem. – Eur. J.*, 2014, **20**, 15280–15291.
17 M. Prongjit, J. Sucharitakul, B. A. Palfey and P. Chaiyen, *Biochemistry*, 2013, **52**, 1437–1445.
18 T. Akiyama, F. Simeno, M. Murakami and F. Yoneda, *J. Am. Chem. Soc.*, 1992, **114**, 6613–6620.
19 B. D. Zoltowski, A. I. Nash and K. H. Gardner, *Biochemistry*, 2011, **50**, 8771–8779.
20 V. Nandwana, I. Samuel, G. Cooke and V. M. Rotello, *Acc. Chem. Res.*, 2013, **46**, 1000–1009.
21 S. Gozem, E. Mirzakulova, I. Schapiro, F. Melaccio, K. D. Glusac and M. Olivucci, *Angew. Chem., Int. Ed.*, 2014, **53**, 9870–9875.
22 M. Szymański, A. Maciejewski and R. P. Steer, *Chem. Phys.*, 1988, **124**, 143–154.
23 S. Sayin, G. Uysal Akkuş, R. Cibulka, I. Stibor and M. Yilmaz, *Helv. Chim. Acta*, 2011, **94**, 481–486.
24 Y.-M. Legrand, M. Gray, G. Cooke and V. M. Rotello, *J. Am. Chem. Soc.*, 2003, **125**, 15789–15795.
25 R. F. Pauszek, G. Kodali, S. T. Caldwell, B. Fitzpatrick, N. Y. Zainalabdeen, G. Cooke, V. M. Rotello and R. J. Stanley, *J. Phys. Chem. B*, 2013, **117**, 15684–15694.
26 F. L. Carter, R. F. Siatkowski and J. Wohltjen, *Molecular Electronic Devices*, Elsevier, Amsterdam, The Netherlands, 1988.
27 J. Jortner and M. A. Ratner, *Molecular Electronics*, Blackwell, Oxford, 1997.
28 L. Crovetto and S. E. Braslavsky, *J. Phys. Chem. A*, 2006, **110**, 7307–7315.
29 F. Tanaka, H. Chosrowjan, S. Taniguchi, N. Mataga, K. Sato, Y. Nishina and K. Shiga, *J. Phys. Chem. B*, 2007, **111**, 5694–5699.
30 Modified flavins with bathochromic absorption may be of interest for neurobiology. R. H. Kramer, D. L. Fortin and D. Trauner, *Curr. Opin. Neurobiol.*, 2009, **19**, 544–552.
31 C. M. Marian, S. Nakagawa, V. Rai-Constapel, B. Karasulu and W. Thiel, *J. Phys. Chem. B*, 2014, **118**, 1743–1753.
32 H. Lettre and M.-E. Fernholz, *Ber. Dtsch. Chem. Ges. B*, 1940, 436–441.
33 A. Rosler and W. Pfleiderer, *Helv. Chim. Acta*, 1997, **80**, 1869–1881.
34 J. Louie and J. F. Hartwig, *Tetrahedron Lett.*, 1995, **36**, 3609–3612.
35 D. Kumar and K. R. J. Thomas, *J. Photochem. Photobiol., A*, 2011, **218**, 162–173.
36 C. Reichardt, *Angew. Chem., Int. Ed. Engl.*, 1979, **18**, 98–110.
37 H. Lettre and M. Fernholz, *Ber. Dtsch Chem. Ges. B*, 1940, 436.
38 A. Niemz, J. Imbriglio and V. M. Rotello, *J. Am. Chem. Soc.*, 1997, **119**, 887–892.
39 S. L. J. Tan and R. D. Webster, *J. Am. Chem. Soc.*, 2012, **134**, 5954–5964.
40 M. J. Frisch, G. W. Trucks, H. B. Schlegel, G. E. Scuseria, M. A. Robb, J. R. Cheeseman, G. Scalmani, V. Barone, B. Mennucci, G. A. Petersson, H. Nakatsuji, M. Caricato, X. Li, H. P. Hratchian, A. F. Izmaylov, J. Bloino, G. Zheng, J. L. Sonnenberg, M. Hada, M. Ehara, K. Toyota, R. Fukuda, J. Hasegawa, M. Ishida, T. Nakajima, Y. Honda, O. Kitao, H. Nakai, T. Vreven, J. A. Montgomery, Jr., J. E. Peralta, F. Ogliaro, M. Bearpark, J. J. Heyd, E. Brothers, K. N. Kudin, V. N. Staroverov, R. Kobayashi, J. Normand, K. Raghavachari, A. Rendell, J. C. Burant, S. S. Iyengar, J. Tomasi, M. Cossi, N. Rega, J. M. Millam, M. Klene, J. E. Knox, J. B. Cross, V. Bakken, C. Adamo, J. Jaramillo, R. Gomperts, R. E. Stratmann, O. Yazyev, A. J. Austin, R. Cammi, C. Pomelli, J. W. Ochterski, R. L. Martin, K. Morokuma, V. G. Zakrzewski, G. A. Voth, P. Salvador, J. J. Dannenberg, S. Dapprich, A. D. Daniels, Ö. Farkas, J. B. Foresman, J. V. Ortiz, J. Cioslowski and D. J. Fox, *Gaussian 09, Revision D.01*, Gaussian, Inc., Wallingford CT, 2009.
41 F. Weigend and R. Ahlrichs, *Phys. Chem. Chem. Phys.*, 2005, **7**, 3297–3305.
42 A. D. Becke, *J. Chem. Phys.*, 1993, **98**, 5648–5652.
43 W. J. Hehre, R. Ditchfield and J. A. Pople, *J. Chem. Phys.*, 1972, **56**, 2257–2261.
44 J. D. Dill and J. A. Pople, *J. Chem. Phys.*, 1975, **62**, 2921–2923.

